



Article

Expression of Melatonin and Dopamine D₃ Receptor Heteromers in Eye Ciliary Body Epithelial Cells and Negative Correlation with Ocular Hypertension

Irene Reyes-Resina ^{1,2,3,*}, Hanan Awad Alkozi ⁴, Anna del Ser-Badia ^{3,5}, Juan Sánchez-Naves ⁶ ,
Jaume Lillo ^{1,3}, Jasmina Jiménez ³, Jesús Pintor ⁴, Gemma Navarro ^{3,7,*} and Rafael Franco ^{3,8,*} 

¹ Department of Biochemistry and Molecular Biomedicine, School of Biology, Universitat de Barcelona, 08028 Barcelona, Spain; lillojaume@gmail.com

² Neuroplasticity Research Group, Leibniz Institute for Neurobiology, 39118 Magdeburg, Germany

³ Centro de Investigación en Red, Enfermedades Neurodegenerativas, CiberNed, Instituto de Salud Carlos III, 28029 Madrid, Spain; delserbadia@gmail.com (A.d.S.-B.); jasminajc@gmail.com (J.J.)

⁴ Department of Biochemistry and Molecular Biology, Faculty of Optics and Optometry, University Complutense of Madrid, 28037 Madrid, Spain; hanan-q1@live.com (H.A.A.); jpintor@ucm.es (J.P.)

⁵ Departament de Bioquímica i Biologia Molecular, Institut de Neurociències, Universitat Autònoma de Barcelona, Cerdanyola del Vallès, 08193 Barcelona, Spain

⁶ Department of Ophthalmology, Balearic Islands Institute of Ophthalmology, 07013 Palma de Mallorca, Mallorca, Spain; juansanchez.naves@gmail.com

⁷ Department of Biochemistry and Physiology, School of Pharmacy and Food Sciences, Universitat de Barcelona, 08027 Barcelona, Spain

⁸ School of Chemistry, Universitat de Barcelona, 08028 Barcelona, Spain

* Correspondence: ire-reyes@hotmail.com (I.R.-R.); g.navarro@ub.edu (G.N.); rfranco123@gmail.com or rfranco@ub.edu (R.F.); Tel.: +34-934021208 (I.R.-R. & G.N.)

Received: 20 November 2019; Accepted: 2 January 2020; Published: 8 January 2020



Abstract: Background: Experiments in the late nineties showed an inverse relationship in the eye levels of melatonin and dopamine, thereby constituting an example of eye parameters that are prone to circadian variations. The underlying mechanisms are not known but these relevant molecules act via specific cell surface dopamine and melatonin receptors. This study investigated whether these receptors formed heteromers whose function impact on eye physiology. We performed biophysical assays to identify interactions in heterologous systems. Particular heteromer functionality was detected using Gi coupling, MAPK activation, and label-free assays. The expression of the heteroreceptor complexes was assessed using proximity ligation assays in cells producing the aqueous humor and human eye samples. Dopamine D₃ receptors (D₃Rs) were identified in eye ciliary body epithelial cells. We discovered heteromers formed by D₃R and either MT₁ (MT₁R) or MT₂ (MT₂R) melatonin receptors. Heteromerization led to the blockade of D₃R-Gi coupling and regulation of signaling to the MAPK pathway. Heteromer expression was negatively correlated with intraocular hypertension. Conclusions: Heteromers likely mediate melatonin and dopamine actions in structures regulating intraocular pressure. Significant expression of D₃R–MT₁R and D₃R–MT₂R was associated with normotensive conditions, whereas expression diminished in a cell model of hypertension. A clear trend of expression reduction was observed in samples from glaucoma cases. The trend was marked but no statistical analysis was possible as the number of available eyes was 2.

Keywords: circadian rhythm; glaucoma; G-protein-coupled receptor GPCR heteromer; melatonin MT₁ and MT₂ receptors; G protein coupling; mitogen-activated protein kinase pathway (MAPK); label-free dynamic mass redistribution (DMR); retina; human 59HCE cells

1. Introduction

The ciliary body, hidden behind the iris, is a complex, highly specialized tissue with a surface containing a series of radially arranged structures known as ciliary processes [1], which are densely vascularized and covered by highly active secretory cells to comply with the function of ciliary processes, i.e., aqueous humor production [2].

The aqueous humor is a clear transparent fluid which bathes the anterior and posterior chambers of the eye [3–5]. It participates in numerous functions such as providing nutrients to the cornea, lens, and trabecular meshwork. More importantly, it also contributes to keeping the force that supports intraocular tissue, thereby giving the eye a certain intraocular pressure (IOP) [6]. IOP is maintained within normal values through a dynamic balance between its constant production by the ciliary processes and its drainage. A lack of balance in the aqueous humor dynamics, usually leading to an increment of IOP, is a significant risk factor in specific ocular pathologies such as glaucoma, the second leading cause of blindness worldwide [7].

Several factors contribute to the homeostasis of IOP, among others, the episcleral vein pressure, the ratio between production and drainage of aqueous humor, the influence of hormones, the innervation by cranial nerves V and VII, and the circadian rhythm. Evidence showed that IOP follows variations throughout the day, being maximal in the early morning and reaching its minimal levels during the night [8]. These fluctuations are small, between 3–5 mm Hg, in healthy subjects. However, they are significantly higher in the glaucomatous eye [9]. The primary modulator of eye circadian rhythms seems to be melatonin.

Melatonin, an indoleamine that participates in the control of circadian rhythms, is a neurohormone first identified in the pineal gland. However, a decade after its discovery by the dermatologist Aaron Lerner and colleagues [10], it gained particular interest because of its multifunctional role. Apart from being synthesized out of the pineal gland, melatonin is also considered an antioxidant and it contributes to minimize the circadian disruption resulting from jet lag or in shift workers [11,12]. Melatonin is synthesized by the retina [13] but, in subsequent studies, other sources were detected, namely, the iris, the ciliary body [14], the crystalline lens [15,16], the Harderian gland [17] and the lacrimal gland [18]. It seems that melatonin can function directly as a free radical scavenger, but it mainly acts via specific cell surface melatonin receptors.

In mammals, two melatonin receptors, MT₁ (MT₁R) and MT₂ (MT₂R) have been cloned and characterized [19,20]. These receptors are present in numerous ocular structures; for instance, they are expressed in the cornea, and among other functions, they accelerate corneal wound healing [21,22]. They mediate regulation of circadian rhythms and neuroendocrine processes in the retina and in the non-pigmented ciliary body epithelium, which mediates IOP control (see References [23,24] and references therein).

Melatonin receptors are members of the 7-transmembrane G protein-coupled receptor family (GPCRs). Both MT₁ and MT₂ receptors belong to the class A of rhodopsin-like GPCRs (<https://gpcrdb.org/>) and contain seven hydrophobic transmembrane helices. Melatonin receptors have a well-established canonical signaling pathway, where the stimulation of MT₁R and MT₂R results in adenylate cyclase (AC) and protein kinase A inactivation by Gi-coupling [25–27]. However, it has been reported that, depending on the tissue or the species studied, melatonin receptors could couple to other G proteins to, for instance, activate phospholipase C- α (PLC α) [28] or inhibit guanylate cyclase (GC) [29]. Interestingly, studies show that the activation of melatonin receptors in the ciliary processes would lead to an increase in cAMP levels [30]. Other possibilities include the influence derived from interactions between these receptors and other receptors or other non-receptor proteins [31]. In this sense, direct interactions between melatonin receptors and GPR50 have been reported. This orphan GPCR may directly interact with the two melatonin receptors, although the interaction does not alter MT₂R but MT₁R coupling to Gi [32]. The MT₂R also interacts directly with 5-hydroxytryptamine 5HT_{2c} receptors, the heteromer leading to biased agonism for the melatonin receptor ligand, agomelatine [33]. Although little is known about melatonin receptor heteromerization in the eye, a recent report has demonstrated

the heteromerization of melatonin and α_1 -adrenergic receptors that alters canonical coupling as heteromerization impedes coupling to the cognate G proteins, Gi and Gq, respectively [26,34].

Dopamine is present in eye structures, and the extracellular level of this neurotransmitter regulates the synthesis of melatonin (in the eye) via dopamine receptors and cAMP as a second messenger [35–38]. The first evidence of an inverse correlation between dopamine and melatonin was found in the pigeon eye. Microdialysis assays found that dopamine concentration decreased when melatonin levels increased. In addition, melatonin injection suppressed the release of dopamine. Subsequent studies in the same laboratory confirmed that melatonin/dopamine interactions were complex but relevant for circadian rhythms in the eye [39,40]. However, the mechanisms underlying dopamine–melatonin relationships in the eye have not yet been elucidated.

Dopamine receptors are grouped into two subfamilies: D₁-like, which includes D₁ and D₅, and D₂-like, which includes D₂, D₃, and D₄ [26]. Dopamine receptor expression has been addressed directly in the retina. Dopamine D₄ receptors were detected in the vertebrate retina [41] and D₂ and D₃ receptors were identified in the human retina by targeted mass spectrometry and positron emission tomography [42]. Indirect evidence based on pharmacological assays and on responses in D₃ receptor (D₃R) KO mice showed that D₃R activation leads to IOP reduction [43–45]. In preliminary experiments, we have detected the D₃ receptor in human ciliary body epithelial cells. The present work aimed to address the potential interaction between dopamine D₃ and melatonin receptors, along with the functional consequences of these interactions. The expressions of D₃R–MT₁R and D₃R–MT₂R heteroreceptor complexes were quantified in a ciliary body-based cell model of elevated IOP, and they were assessed in samples from human normotensive and hypertensive eyes. The results proved heteromerization and provided evidence of a negative correlation between ocular hypertension and heteromer expression.

2. Materials and Methods

This work adhered to the guidelines detailed in Reference [46] and to the Helsinki declaration regarding the ethics of working with human samples. The studies were designed to generate groups of equal size, using randomization and blinded analysis. Immuno-based assays were conducted in line with guidelines detailed in Alexander et al., 2018 [47].

2.1. Drugs

(RS)-*trans*-7-Hydroxy-2-[N-propyl-N-(3'-iodo-2'-propenyl)amino]tetralin (7-OH-PIPAT) maleate (mixed D₂R/D₃R agonist), 3,5-Dichloro-N-[[2(2S)-1-ethyl-2-pyrrolidinyl]methyl]-2-hydroxy-6-methoxybenzamide (raclopride: D₃R antagonist), N-Acetyl-5-methoxytryptamine (melatonin), N-*o*-cetyl-2-benzyltryptamine (luzindole: non-selective MTR antagonist), N-[(1S)-1-[[4-[(2S)-2-[(2,4-dichlorophenyl)sulfonyl]amino]-3-hydroxy-1-oxopropyl]-1-piperazinyl]carbonyl]-3-methylbutyl]benzo[b]thiophene-2-carboxamide (GSK1016790A: selective TRPV4 agonist), and cis-4-phenyl-2-propionamidotetralin (4PPDOT, a selective MT₂R antagonist) were purchased from Tocris Bioscience (Bristol, UK). N-[2-(2-methoxy-6H-isoindolo[2,1-a]indol-11-yl)ethyl]butanamide (IHK7, a selective MT₂ receptor agonist [48]) was purchased from Sigma-Aldrich (St. Louis, MO, USA).

2.2. Cell Culture and Transient Transfection

A human non-pigmented ciliary epithelial (59HCE) immortalized cell line was supplied by Dr. Coca-Prados (Yale University). Cells were grown in high glucose Dulbecco's modified Eagle's medium (Gibco/Invitrogen, Carlsbad, CA) containing 10% fetal bovine serum (Sigma-Aldrich, St. Louis, MO, USA) and 0.05 mg/mL penicillin/streptomycin (Gibco/Invitrogen) at 37 °C in a humidified atmosphere of 5% CO₂. After the culture reached the confluence, the cells were detached with 0.25% trypsin and seeded into 6 well plates or glass coverslips. All the experiments were performed using cells under 10–15 passages to assure assay reproducibility. Then, 59HCE cells were treated with a selective

TRPV4 agonist, GSK1016790A (1–10,000 nM range), over 18 h, for the performance of the proximity ligation assay.

HEK-293T cells grown in DMEM (Gibco/Invitrogen, Carlsbad, CA, USA) were processed as previously described in References [49,50]. Briefly, HEK-293T cells growing in 6-well dishes were transfected transiently with the corresponding cDNA using the PEI (PolyEthylenImine, Sigma-Aldrich, St. Louis, MO, USA) method. The cells were incubated (for 4h) with the corresponding cDNA together with PEI (5.47 mM in nitrogen residues) and 150 mM NaCl in a serum-starved medium. After 4 h, the medium was replaced by a fresh complete culture medium.

2.3. Fusion Proteins and Expression Vectors

The human cDNAs for the D₃, MT₁, MT₂, and GHS-R1a receptors cloned in pcDNA3.1 were amplified without their stop codons using sense and antisense primers. The primers harbored either unique BamHI and HindIII sites for D₃; EcoRI and KpnI sites for GHS-R1a or Hind III; and BamHI sites for MT₁ and MT₂. The fragments were subcloned to be in frame with an enhanced yellow fluorescent protein (pEYFP-N1; Clontech, Heidelberg, Germany) or an Rluc (pRluc-N1; PerkinElmer, Wellesley, MA) on the C-terminal end of the receptor to produce D₃-RLuc, MT₁-YFP, MT₂-YFP and GHS-R1a-YFP fusion proteins.

2.4. Bioluminescence Resonance Energy Transfer (BRET) Assays

HEK-293T cells growing in 6-well plates were transiently co-transfected with a constant amount of cDNA encoding for D₃R fused to Renilla luciferase (D₃-Rluc) and with increasing amounts of cDNAs corresponding to MT₁R, MT₂R or ghrelin receptor GHS-R1a fused to the yellow fluorescent protein (MT₁-YFP, MT₂-YFP, GHS-R1a-YFP). 48 h post-transfection cells were washed twice in quick succession in HBSS (137 mM NaCl; 5 mM KCl; 0.34 mM Na₂HPO₄; 0.44 mM KH₂PO₄; 1.26 mM CaCl₂; 0.4 mM MgSO₄; 0.5 mM MgCl₂ and 10 mM HEPES, pH 7.4) supplemented with 0.1% glucose (w/v), detached by gently pipetting and resuspended in the same buffer. To assess the number of cells per plate, we determined protein concentration using a Bradford assay kit (Bio-Rad, Munich, Germany) with bovine serum albumin dilutions as standards. To quantify YFP-fluorescence expression, we distributed the cells (20 µg protein) in 96-well microplates (black plates with a transparent bottom; Porvair, Leatherhead, UK). Fluorescence was read using a Mithras LB 940 (Berthold, Bad Wildbad, Germany) equipped with a high-energy xenon flash lamp, using a 10-nm bandwidth excitation and emission filters at 485 and 530 nm, respectively. YFP-fluorescence expression was determined as the fluorescence of the sample minus the fluorescence of cells expressing protein-Rluc alone. For the BRET measurements, the equivalent of 20 µg of cell suspension was distributed in 96-well microplates (white plates; Porvair), and we added 5 µM coelenterazine H (PJK GMBH, Kleinblittersdorf, Germany). Then, 1 min after coelenterazine H addition, the readings were collected using a Mithras LB 940 (Berthold, Bad Wildbad, Germany), which allowed the integration of the signals detected in the short-wavelength filter at 485 nm (440–500 nm) and the long-wavelength filter at 530 nm (510–590 nm). To quantify receptor-Rluc expression, we performed luminescence readings 10 min after addition of 5 µM coelenterazine H. The net BRET is defined as [(long-wavelength emission)/(short-wavelength emission)]-Cf where Cf corresponds to [(long-wavelength emission)/(short-wavelength emission)] for the Rluc construct expressed alone in the same experiment. The BRET curves were fitted assuming a single phase by a non-linear regression equation using the GraphPad Prism software (San Diego, CA, USA). BRET values are given as milli BRET units (mBU: 1000 × net BRET).

2.5. cAMP Level Determination

Two hours before initiating the experiment, 59HCE cells or HEK-293T cell-culture medium were exchanged to serum-starved DMEM medium. Then, the cells were detached, re-suspended in growing medium containing 50 µM zardaverine, and plated in 384-well microplates (2500 cells/well), pretreated (15 min) with the corresponding antagonists—or vehicle—and stimulated with agonists (15 min)

before adding 0.5 μ M forskolin or vehicle. Readings were performed after 1 h incubation at 25 °C. Homogeneous time-resolved fluorescence energy transfer (HTRF) measures were obtained using the Lance Ultra cAMP kit (PerkinElmer, Waltham, MA, USA) (see Reference [51]). Fluorescence at 665 nm was analyzed on a PHERAstar Flagship microplate reader equipped with an HTRF optical module (BMG Lab technologies, Offenburg, Germany).

2.6. Extracellular Signal-Regulated Kinase Phosphorylation Assays

To determine extracellular signal-regulated kinase 1/2 (ERK1/2) phosphorylation, 40,000 59HCE or HEK-293T cells/well were plated in transparent Deltalab 96-well plates and kept in the incubator for 48 h. Then, 2 to 4 h before the experiment the medium was replaced by serum-free medium. The cells were pre-treated at 25 °C for 10 min with antagonists or vehicle and stimulated for an additional 7 min with selective agonists. The cells were then washed twice with cold PBS before the addition of lysis buffer (a 20 min treatment). Afterward, 10 μ L of each supernatant were placed in white ProxiPlate 384-well plates and ERK 1/2 phosphorylation was determined using an AlphaScreen[®]SureFire[®] kit (Perkin Elmer), following the instructions of the supplier, and using an EnSpire[®] Multimode Plate Reader (PerkinElmer, Waltham, MA, USA). The value of reference (100%) was the value achieved in the absence of any treatment (basal). The effect of ligands was given in percentage with respect to the basal value.

2.7. Label-Free Dynamic Mass Redistribution (DMR) Assay

Cell mass redistribution induced upon receptor activation was detected by illuminating the underside of a biosensor with polychromatic light. We then measured the changes in the wavelength of the reflected monochromatic light, which is a sensitive function of the index of refraction. The magnitude of the wavelength shift (in picometers) is directly proportional to the amount of mass redistribution. HEK-293T or 59HCE cells were seeded in 384-well sensor microplates to obtain 70–80% confluent monolayers constituted by approximately 10,000 cells per well. Previous to the assay, the cells were washed twice with assay buffer (HBSS with 20 mM HEPES, pH 7.15) and incubated for 2 h with assay-buffer containing 0.1% DMSO (24 °C, 30 μ L/well). Hereafter, the sensor plate was scanned, and a baseline optical signature was recorded for 10 min before adding 10 μ L of the selective antagonists for 30 min, followed by the addition of 10 μ L of the selective agonists. All test compounds were dissolved in assay buffer. Then, DMR responses elicited by the agonists were monitored for at least 5000 s in an EnSpire[®] Multimode Plate Reader (PerkinElmer, Waltham, MA, USA). The results were analyzed using EnSpire Workstation software v 4.10.

2.8. Human Eye Postmortem Samples

Donor human eyes were obtained from the Fundación Banco de Sangre y Tejidos de las Islas Baleares (Balearic Islands Blood and Tissue Bank). This biobank is supervised by the regional Balearic Islands Government, which is in charge of enforcing the principles in Helsinki declaration. All donations are made after appropriate filling and signing of informed consent by patients or their legal representatives. Two eyes of healthy normal subjects and two of glaucoma patients were used for the assays. The eyes were enucleated and collected without the cornea in sterile tubes and maintained in 4% paraformaldehyde in 0.1 M phosphate buffer (PB) (pH 7.2–7.4) at 4 °C until posterior processing. Eyes were dissected under a stereomicroscope (Zeiss), with a 0.8 mm curved tip forceps and sterile dissecting scissors, where we collected the iris and ciliary processes. Several washes in PBS were performed, and then, the specimens were cryoprotected in a sucrose gradient (from 11% to 33%) and embedded in tissue freezing medium (Tissue-Tek[®] OCT) until frozen with liquid N₂. Vertical sections of control and glaucomatous human samples (10 μ m thick) were collected using a cryostat (Leica, Nussloch, Germany) and were mounted from the same region. The samples were maintained at –20 °C until use.

2.9. Immunofluorescence Studies

HEK-293T cells were fixed in 4% paraformaldehyde for 15 min and then washed twice with PBS containing 20 mM glycine before permeabilization with the same buffer containing 0.2% Triton X-100 (5 min incubation). The cells were treated for 1 h with PBS containing 1% bovine serum albumin and labeled with a mouse anti-Rluc (1/100; MAB4400, Millipore) antibody and subsequently treated with Cy3-conjugated anti-mouse (1/200; 715-166-150; Jackson ImmunoResearch (red)) IgG secondary antibody (1 h each). Alternatively, cells were labeled with rabbit anti-D₃R (#ab42114), anti-MT₁R (#ab203038), or anti-MT₂R (#ab115336) antibodies, all from Abcam (Cambridge, UK) and subsequently treated with Cy3-conjugated anti-rabbit (1/200; #711-166-152; Jackson ImmunoResearch (red)) IgG secondary antibody (1 h each). The samples were washed several times and mounted with 30% Mowiol (Calbiochem). Samples were observed under a Leica SP2 confocal microscope (Leica Microsystems).

2.10. In Situ and In Vitro Proximity Ligation Assay (PLA)

The proximity ligation assay (PLA) allows the detection of molecular interactions between two endogenous proteins *ex vivo*. PLA requires both receptors to be sufficiently close (<16 nm) to allow double-strand formation of the complementary DNA probes conjugated to the antibodies. Using the PLA, the heteromerization of D₃R with MT₁ and MT₂ receptors was detected in non-pigmented epithelial ciliary body cells (59HCE) and, *in situ*, in the human ciliary body sections of healthy and glaucomatous donors.

The presence/absence of receptor–receptor molecular interactions in the samples was detected using the Duolink II In Situ PLA Detection Kit (developed by Olink Bioscience, Uppsala, Sweden; and now distributed by Sigma-Aldrich as Duolink[®] using PLA[®] Technology). The PLA probes were obtained after conjugation of the primary anti-D₃R antibody (ab42114, Abcam, Cambridge, UK) to a PLUS oligonucleotide (DUO92009, Sigma-Aldrich, St. Louis, MO, USA), and the anti-MT₁R (ab203038, Abcam, Cambridge, UK) and -MT₂R (ab115336, Abcam, Cambridge, UK) antibodies to a MINUS oligonucleotide (DUO92010, Sigma-Aldrich, St. Louis, MO, USA). The specificity of antibodies was tested in non-transfected HEK-293T cells (see Appendix A Figure A3). Samples were fixed in 4% paraformaldehyde for 15 min and then washed twice with PBS containing 20 mM glycine before permeabilization with PBS-glycine containing 0.2% Triton X-100 (5 min incubation for the 59HCE cells and 15 min for the ciliary body sections). After permeabilization, the samples were washed in PBS at room temperature and incubated in a preheated humidity chamber for 1 h at 37 °C with the blocking solution provided in the PLA kit. Then, the samples were incubated overnight with the PLA probe-linked antibodies (1:100 dilution for all antibodies) at 4 °C. After washing, the samples were incubated with the ligation solution for 1 h, and then washed and subsequently incubated with the amplification solution for 100 min (both steps at 37 °C in a humid chamber). Nuclei were stained with Hoechst (1/100; Sigma-Aldrich, St. Louis, MO, USA). Mounting was performed using 30% Mowiol (Calbiochem). Negative controls were performed by omitting the anti-D₃R-PLUS antibody. Samples were observed using a Leica SP2 confocal microscope (Leica Microsystems, Mannheim, Germany) equipped with an apochromatic 63× oil-immersion objective (N.A. 1.4), and with 405 nm and 561 nm laser lines. For each field of view, we acquired a stack of two channels (one per staining) and 5 Z planes with a step size of 1 μm. The ratio *r* (number of red spots/cell) was determined on the maximum projection of each image stack using the Duolink Image tool software.

2.11. Data Analysis

Data, expressed as the mean ± SEM, were obtained from at least five independent experiments. Data comparisons were analyzed by one-way ANOVA or two-way ANOVA, followed by Bonferroni's post-hoc test. The normality of populations and homogeneity of variances were tested before the ANOVA. Statistical analysis was undertaken only when each group size was at least *n* = 5, *n* being the number of independent variables (technical replicates were not treated as independent variables).

Differences were considered significant when $P \leq 0.05$. Statistical analyses were carried out with GraphPad Prism software version 5 (San Diego, CA, USA). Outliers tests were not used, and all data points (mean of replicates) were used for the analyses.

3. Results

3.1. Dopamine D_3 Receptors Interact with Melatonin MT_1 Receptors in the HEK-293T Cells

To determine whether the dopamine D_3 receptor (D_3R) could interact with the melatonin MT_1 receptor, we first performed immunocytochemical assays in a heterologous expression system. HEK-293T cells were transfected with cDNAs coding for D_3R -Rluc or MT_1R -YFP. Expression of D_3R -Rluc was detected using an anti-Rluc primary antibody followed by a secondary Cy3-conjugated antibody, and expression of MT_1R -YFP was detected using the YFP's fluorescence. Receptor expression was found in different cell compartments, including the plasma membrane (Appendix A Figure A1A, left and center panels). When the cells were co-expressing D_3R -Rluc and MT_1R -YFP, a significant degree of co-localization was observed (yellow in Figure 1A).

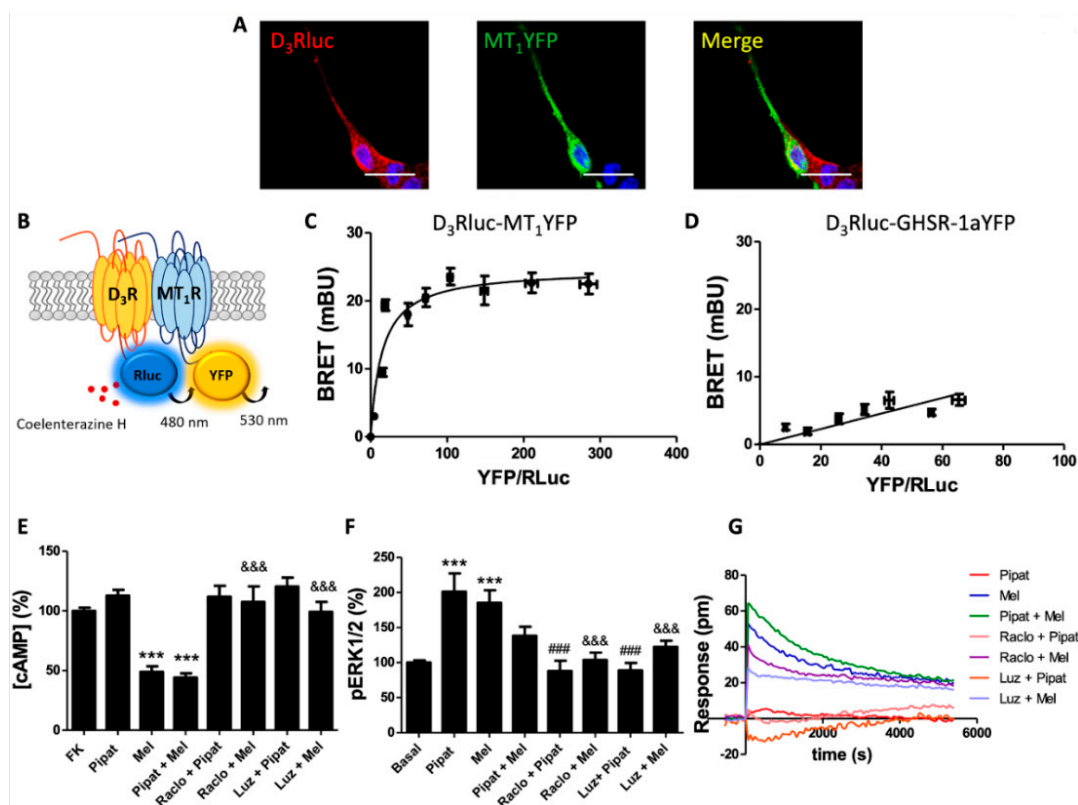


Figure 1. Molecular interaction between D_3 and MT_1 receptors, and heteromer-mediated signaling. (A) Confocal microscopy images of HEK-293T cells co-expressing D_3R -Rluc (2 μ g) and MT_1R -YFP (2 μ g). D_3 receptor (red) was identified by immunocytochemistry using anti-Rluc antibodies. MT_1 receptor (green) was identified from the fluorescence of YFP-containing fusion proteins. Co-localization is shown in the panel on the right (yellow). Cell nuclei were stained with Hoechst (blue channel). Scale bar: 20 μ m. (B) Scheme of the bioluminescence resonance energy transfer (BRET) assay. (C,D) BRET saturation experiments performed using HEK-293T cells co-transfected with D_3R -Rluc cDNA (0.7 μ g) and increasing amounts of MT_1R -YFP cDNA (0–1.4 μ g cDNA) (C) or GHSR-1a-YFP cDNA (0–2.5 μ g cDNA) as a negative control (D). BRET data are expressed as the mean \pm S.D. of 8 different experiments performed in duplicates. mBU: milliBret units. HEK-293T cells transfected with cDNA encoding for D_3R (1 μ g) and MT_1R (1 μ g) were pre-treated or not with receptor antagonists (1 μ M raclopride for D_3R or 1 μ M luzindole for MT_1R) and then subsequently treated with agonists (100 nM 7-OH-PIPAT for

D₃R or 1 μ M melatonin for MT₁R), alone or in combination. (E) cAMP data were expressed as a % over 0.5 μ M forskolin-induced levels. (F) ERK1/2 phosphorylation was analyzed using an AlphaScreen® SureFire® kit (Perkin Elmer). ERK1/2 phosphorylation data are expressed as % with respect to basal levels. In cAMP accumulation and MAPK activation assays, values are the mean \pm S.E.M. of 6 different experiments performed in triplicates. One-way ANOVA followed by Bonferroni's multiple comparison post-hoc tests were used for statistical analysis. (** $p < 0.001$; versus treatment with forskolin in cAMP or basal in pERK assays). (### $p < 0.001$; versus treatment with 7-OH-PIPAT alone). (&&& $p < 0.001$; versus treatment with melatonin alone). (G) label-free dynamic mass redistribution (DMR) tracings are representing the picometer-shifts of reflected light wavelengths over time upon ligand treatment.

As co-localization is not direct evidence of interaction, we used an energy-transfer biophysical approach aimed at identifying direct physical interactions. Bioluminescence resonance energy transfer (BRET) assays were performed in HEK-293T cells expressing a constant amount of D₃R-Rluc and increasing amounts of MT₁R-YFP (Figure 1B). A saturation BRET curve was obtained (BRET_{max} 24.6 mBU, BRET₅₀ 14.9) (Figure 1C), indicating that D₃R and MT₁R physically interacted. As a negative control, D₃R was co-expressed with a non-interacting partner, the ghrelin receptor GHSR-1a. In this case, the cells were co-transfected with a constant amount of D₃R-Rluc and increasing amounts of GHSR-1aYFP. A linear signal was obtained, indicating the lack of interaction between these receptors (Figure 1D). These results indicated that D₃ and MT₁ may form heteroreceptor complexes in a heterologous expression system.

3.2. Functional Characterization of D₃-MT₁ Heteroreceptor Complexes in HEK-293T Cells

Before estimating whether D₃R and MT₁R signaling properties were altered by D₃R–MT₁R heteromerization, we performed assays in single-transfected cells. These preliminary assays consisted of dose-response curves, to select the single agonist concentration for use in further assays performed in cells expressing the two receptors. Cognate heterotrimeric G proteins are Gi/o for melatonin and D₃ receptors [26]. Thus, activation of these receptors leads to a decrease in cytosolic cAMP levels. We have confirmed that this is the case in single transfected cells (Appendix A Figure A1B,C; see also our recent report [52]), thereby reproducing data reported in References [34,53]. HEK-293T cells expressing D₃R or MT₁ and incubated with the selective agonists, 7-OH-PIPAT for D₃ and melatonin for MT₁, led to significant decreases in the forskolin-induced cytosolic cAMP levels. The blockade was afforded by the respective antagonist, raclopride, or luzindole (Appendix A Figure A1B,C). Next, we analyzed the mitogen-activated protein kinase (MAPK) signaling pathway, which may be mediated by G-protein-dependent or independent mechanisms. Experiments performed in single-transfected cells HEK-293T cells expressing D₃R or MT₁R led to a dose-response increase in phosphorylated ERK1/2 levels, which was reversed by the respective antagonists (Appendix A Figure A2A,B). Finally, we used a label-free approach based on the cell's dynamic mass redistribution (DMR). Increasing agonist concentrations were assayed in single-transfected HEK-293T cells expressing D₃R or MT₁R treated with 7-OH-PIPAT or with melatonin, respectively. In both cases, we could observe significant DMR outputs that were reverted by the respective antagonists (Appendix A Figure A2D,E).

Next, HEK-293T cells were transfected with both D₃R and MT₁R and then treated with 100 nM 7-OH-PIPAT and 1 μ M melatonin, alone or in combination. Melatonin induced a decrease in the forskolin-induced cAMP levels to a similar extent to that produced in cells only expressing MT₁R. In contrast, 7-OH-PIPAT did not produce any effect (Figure 1E). These results suggest that the co-expression of MT₁R blocks the 7-OH-PIPAT-induced D₃R activation and Gi-mediated signaling. The effect in simultaneous treatment with agonists was similar to that produced by melatonin alone. When the cells were pre-treated with antagonists, we could observe that the melatonin effect was not only abolished by the MT₁R antagonist, luzindole, but also by the D₃R antagonist, raclopride (Figure 1E). This cross-antagonism, consisting of the antagonist of one receptor blocking the signal of the partner receptor, is often found in GPCR heteroreceptor complexes.

When the MAPK signaling pathway was analyzed in the HEK-293T cells co-expressing D₃ and MT₁ receptors, a significant ERK1/2 phosphorylation was observed when the cells were treated with 7-OH-PIPAT or melatonin. These results showed that MT₁R did not block 7-OH-PIPAT-induced D₃R signaling in the MAPK pathway (Figure 1F). Interestingly, the effect was much lower when the cells were stimulated simultaneously with both agonists. Simultaneous co-activation resulting in reduced signaling is known as negative cross-talk and has been reported for other GPCR heteromers. When cells were pre-treated with antagonists, a bi-directional cross-antagonism was detected, which consisted of the antagonists of either receptor blocking the activation of the partner receptor in the heteromer. Indeed, the D₃R antagonist raclopride inhibited not only the effect of 7-OH-PIPAT but also the effect of melatonin, and the MT₁R antagonist luzindole inhibited the effect of each agonist (Figure 1F).

DMR assays performed in the cells co-expressing D₃R and MT₁R led to results that were similar to those observed in [cAMP] determination assays. While melatonin produced a significant effect on DMR, 7-OH-PIPAT did not produce any effect (Figure 1G). When the cells were pre-treated with antagonists, we observed a cross-antagonism phenomenon, as the melatonin effect was not only inhibited by luzindole, but also by raclopride.

Together, the results showed that the consequences of D₃-MT₁ heteroreceptor complex formation included a blockade of D₃R-Gi coupling, a negative cross-talk in signaling towards the MAPK pathway, and a cross-antagonism.

3.3. Dopamine D₃ Receptors Interact with Melatonin MT₂ Receptors in HEK-293T Cells

We considered the possibility of the D₃R also interacting with the MT₂R. Accordingly, we followed the same strategy described earlier for MT₁R. Immunocytochemical assays showed the presence of the receptor in different cell compartments, including the cell membrane (Appendix A Figure A1A, right). In double-transfected cells, a high degree of co-localization between D₃R and MT₂R was observed (Figure 2A). Next, the BRET assay, schematized in Figure 2B, undoubtedly proved that D₃R might form heteroreceptor complexes with MT₂R in a heterologous expression system. The saturation curve was characterized by a BRET_{max} of 30.7 mBU and a BRET₅₀ of 38.2.

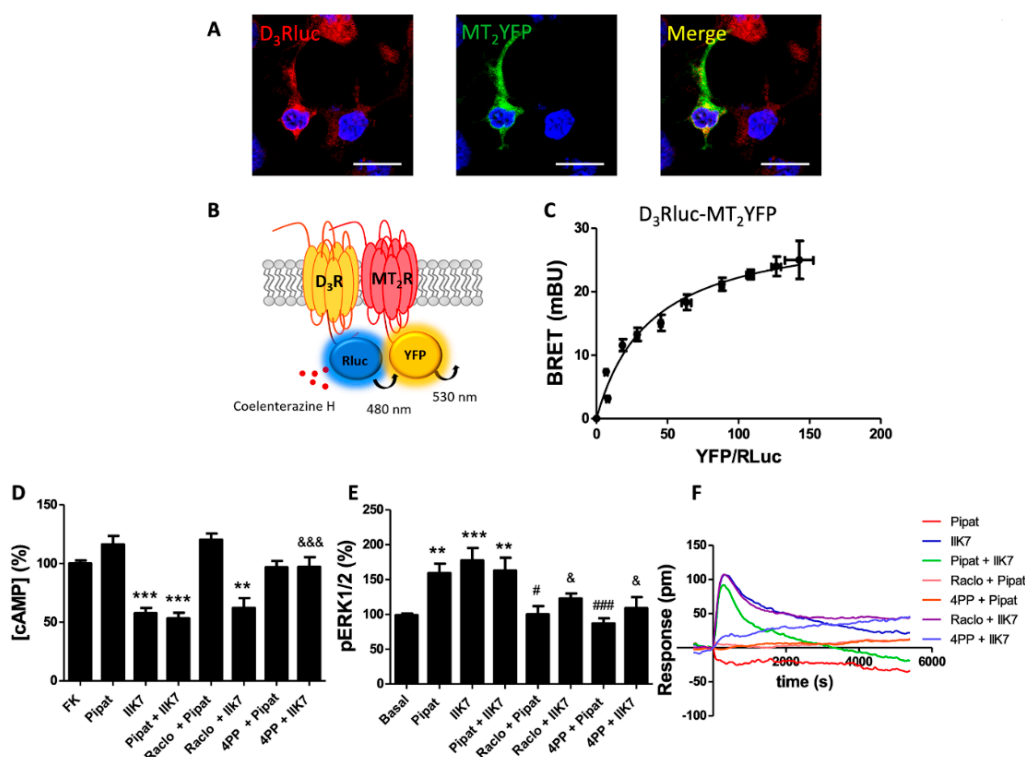


Figure 2. Molecular interaction between D₃ and MT₂ receptors, and heteromer-mediated signaling.

(A) Confocal microscopy images of HEK-293T cells co-expressing D₃R-Rluc (2 µg) and MT₂R-YFP (2 µg). D₃ receptor (red) was identified by immunocytochemistry using anti-Rluc antibodies. MT₂ receptor (green) was identified from the fluorescence of YFP-containing fusion proteins. Co-localization is shown in the panel on the right (yellow). Cell nuclei were stained with Hoechst (blue channel). Scale bar: 20 µm. (B) Scheme of the BRET assay. (C) BRET saturation experiments performed using HEK-293T cells co-transfected with D₃R-Rluc cDNA (0.7 µg) and increasing amounts of MT₂R-YFP cDNA (0–2.3 µg cDNA). BRET data are expressed as the mean ± S.D. of 8 different experiments performed in duplicates. mBU: milliBret units. Panels (D–F) Signaling in HEK-293T cells transfected with cDNA encoding for D₃R (1 µg) and MT₂R (1 µg) were pre-treated with antagonists (1 µM raclopride for D₃R or 1 µM 4PPDOT for MT₂R) or vehicle, and then subsequently treated with selective agonists (100 nM 7-OH-PIPAT for D₃R and 300 nM IIK7 for MT₂R), individually or in combination. (D) [cAMP] (expressed as % with respect to treatment with 0.5 µM forskolin) was detected by TR-FRET. (E) ERK1/2 phosphorylation was analyzed using an AlphaScreen® SureFire® kit (Perkin Elmer). ERK1/2 phosphorylation data are expressed as % with respect to basal levels. In cAMP accumulation and MAPK signaling assays, the values are the mean ± S.E.M. of 6 different experiments performed in triplicates, and one-way ANOVA followed by Bonferroni's multiple comparison post-hoc tests were used for statistical analysis. (** $p < 0.01$, *** $p < 0.001$; versus treatment with forskolin in cAMP or basal in pERK assays). (# $p < 0.05$, ### $p < 0.001$; versus treatment with 7-OH-PIPAT alone). (& $p < 0.05$, && $p < 0.001$; versus treatment with IIK7 alone). (F) DMR tracings representing the picometer-shifts of reflected light wavelengths over time upon ligand treatment.

3.4. Functional Characterization of the D₃-MT₂ Heteroreceptor Complexes in HEK-293T Cells

Dose-response assays in HEK-293T cells expressing MT₂R were performed using a selective MT₂R agonist, IIK7. The results were consistent with Gi coupling, with MAPK activation, and with marked DMR readings. Pretreatment with the MT₂R antagonist 4P-PDOT blocked the MT₂R agonist-induced effect (Appendix A Figures A1D and A2C,F).

In forskolin-pretreated HEK-293T cells co-expressing D₃R and MT₂R, treatment with 7-OH-PIPAT did not decrease cAMP levels, while IIK7 was able to produce a signal similar to that produced in single-transfected cells. This result indicated that co-expression of MT₂R blocks 7-OH-PIPAT-induced Gi-mediated signaling (Figure 2D), in full resemblance to what was observed for the D₃R–MT₁R heteromer. However, for the D₃R–MT₂R heteromer, no cross-antagonism was detected. When activation of the MAPK pathway was analyzed in cotransfected HEK-293T cells, we observed the same phenomena encountered for the D₃R–MT₁R heteromer. Both agonists were able to elicit a signal when used separately but a negative cross-talk was detected in simultaneous co-activation. In this experiment, the bi-directional cross-antagonism effect was observed, as both raclopride and 4P-PDOT were able to block the signal elicited by either D₃R or MT₂R activation (Figure 2E). Finally, when the DMR responses were analyzed, 7-OH-PIPAT did not produce any signal, while IIK7 produced a significant effect. Again, as in the cAMP assays, no cross-antagonism was detected. The IIK7-induced signal was only blocked by MT₂R antagonist 4P-PDOT and not by the D₃R antagonist raclopride. To sum up, the results showed that the consequences of D₃-MT₂ heteroreceptor complex formation included a blockade of D₃R-Gi coupling and a negative cross-talk plus bi-directional cross-antagonism when signaling towards the MAPK pathway was analyzed.

3.5. Detection and Functional Characterization of D₃-MT₁ and D₃-MT₂ Heteroreceptor Complexes in Human Non-Pigmented Ciliary Body Epithelial Cells

To determine whether D₃R–MT₁R and D₃R–MT₂R heteromers occur in natural sources, we took advantage of a technique that allows the detection of clusters of two receptors in fixed cells or tissue sections, i.e., the in situ proximity ligation assay (PLA). The PLA was performed in the non-pigmented human ciliary body epithelial 59HCE cell line, which expresses three receptors. Specific antibodies

against D₃, MT₁, and MT₂ receptors were used (see Appendix A Figure A3) and punctuated red marks were visualized surrounding stained nuclei. This outcome demonstrated the existence of D₃-MT₁ and D₃-MT₂ receptor complexes/clusters (Figure 3A, top and bottom left—0 nM).

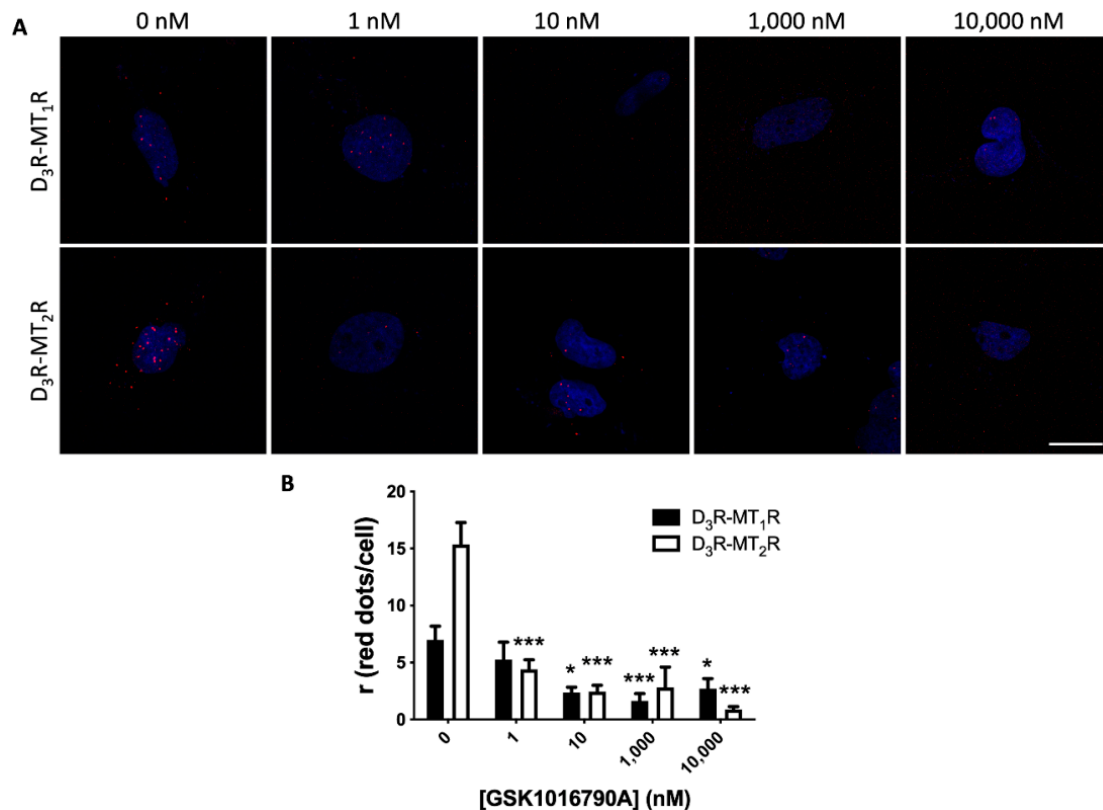


Figure 3. D₃-MT₁ and D₃-MT₂ heteroreceptor expression in human 59HCE cells. Proximity ligation assay (PLA) was performed as described in Methods to detect D₃-MT₁ and D₃-MT₂ receptor complexes in the 59HCE non-pigmented ciliary body epithelial cell line, using specific antibodies against D₃ and either MT₁ or MT₂ receptors. (A) Cells were treated with different concentrations of GSK1016790A, a TRPV4 agonist. Representative images corresponding to stacks of 5 sequential planes are shown. Cell nuclei were stained with Hoechst (blue) and heteroreceptor clusters appear as red dots. (B) Ratio (*r*; number of red spots/cell-containing spots) is the mean ± S.E.M. of counts in 5 different fields from every sample (*n* = 5). One-way ANOVA followed by Bonferroni's multiple comparison post-hoc test were used for statistical analysis. (* *p* < 0.05, *** *p* < 0.001; versus 0 nM GSK1016790A). Scale bar: 20 μm.

Next, we studied the signaling properties of D₃-MT₁ and D₃-MT₂ heteroreceptor complexes in the 59HCE cells using the approaches described in previous subsections. When cytosolic cAMP levels were analyzed in the cells treated with 0.5 μM forskolin, the D₃R agonist 7-OH-PIPAT, in agreement with the heteromer's print identified in the HEK-293T cells, did not produce any effect (Figure 4A,D).

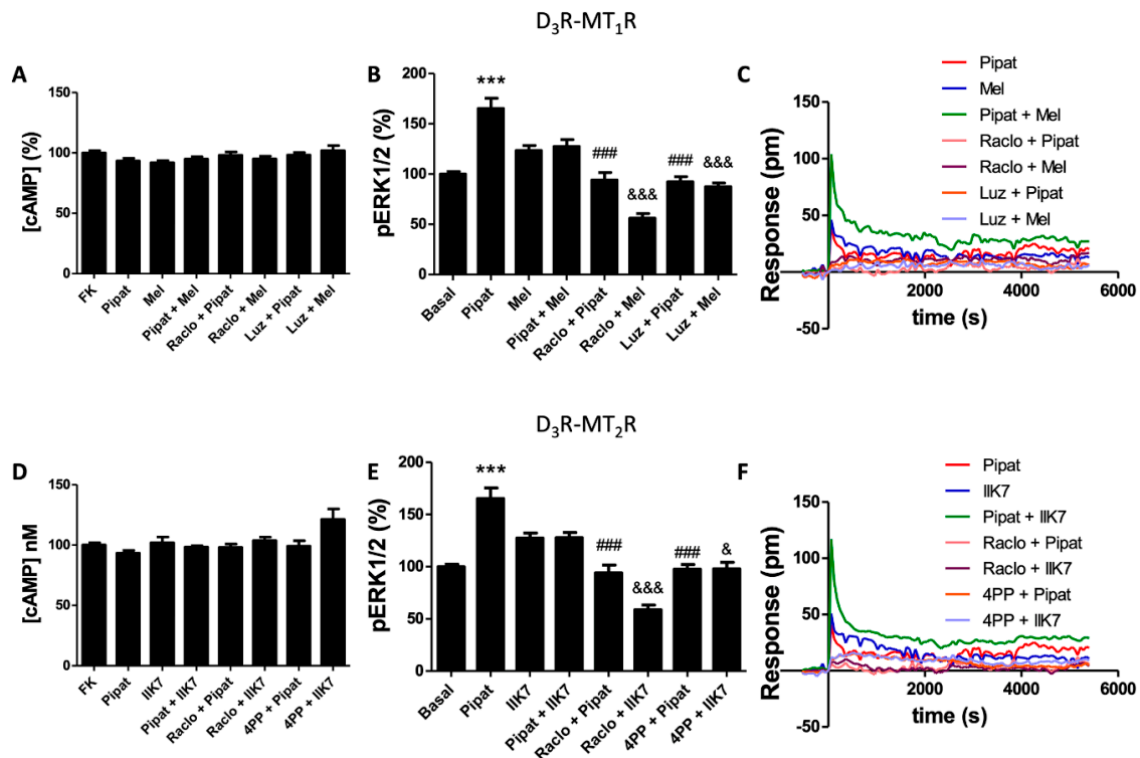


Figure 4. Effect of dopamine and melatonin receptor agonists in human 59HCE cells. Signaling was assayed in the 59HCE cells pre-treated with antagonists (1 μ M raclopride for D₃R, 1 μ M luzindole for MT₁R, or 1 μ M 4PPDOT for MT₂R) or vehicle, and then subsequently treated with agonists (100 nM 7-OH-PIPAT for D₃R and either 1 μ M melatonin for MT₁R (A–C) or 300 nM I1K7 for MT₂R (D–F)), individually or in combination. (A,D) cAMP production is expressed as % over 0.5 μ M forskolin-induced [cAMP] increases. (B,E) ERK1/2 phosphorylation data are expressed as % with respect to basal levels. In cAMP accumulation and MAPK signaling assays, the values are the mean \pm S.E.M. of 5 different experiments performed in triplicates, and one-way ANOVA followed by Bonferroni's multiple comparison post-hoc tests were used for statistical analysis. (***) $p < 0.001$; versus basal in pERK assays). (###) $p < 0.001$; versus treatment with 7-OH-PIPAT alone). (& $p < 0.05$, &&& $p < 0.001$; versus treatment with melatonin or I1K7 alone). (C,F) DMR tracings representing the picometer-shifts of reflected light wavelengths over time upon ligand treatment. Note that data related to D₃R agonists are the same in the upper and lower panels; for clarity, we decided to keep six panels instead of including all the information in three panels.

Interestingly, and as previously described by Alkozi et al., [34], none of the melatonin receptor agonists, melatonin or I1K7, were able to decrease cAMP levels in these cells. Next, we analyzed ERK1/2 phosphorylation, which was significantly enhanced when 7-OH-PIPAT was added (Figure 4B,E). When the cells were treated with 7-OH-PIPAT in combination with melatonin or with I1K7, a negative cross-talk was observed, whereas a bi-directional cross antagonism occurred for both the D₃R–MT₁R and D₃R–MT₂R heteromers. Finally, interpretation of the DMR data resulting from activation of the receptors in the two heteromers was complex (Figure 4C,F). Perhaps the most relevant finding was the bi-directional cross-antagonism detected for both D₃R–MT₁R and D₃R–MT₂R heteromers expressed in the 59HCE cells. Apart from the evidence on heteromer formation, the results showed that neither D₃, MT₁, or MT₂ receptors were coupled functionally to Gi and that D₃R–MT₁R and D₃R–MT₂R signaling was biased towards the MAPK pathway.

3.6. Differential Expression of D₃-MT₁ and D₃-MT₂ Heteroreceptor Complexes in the Glaucomatous Eye

We wondered whether intraocular hypertension correlated with the altered expression of dopamine and melatonin heteroreceptor complexes. First of all, we took advantage of an in vitro model of

hypertension, described in Reference [54], consisting of the activation of the transient receptor potential vanilloid 4 (TRPV4) channel. Such activation in 59HCE cells using GSK1016790A mimics the ion fluxes that drive the increase in hydrostatic pressure that occurs in the hypertensive/glaucomatous eye. TRPV4 stimulation by application of the agonist, GSK1016790A, was followed by PLA to detect the D₃R-containing heteromers. Remarkably, increasing GSK1016790A concentrations translated into a significant decrease in the PLA signal for D₃R–MT₁ and D₃R–MT₂ heteromers, and the effect was dose-dependent. The reduction was up to 45% for D₃R–MT₁R heteromer expression, and up to 95% in the case of D₃R–MT₂R heteromers (Figure 3A,B). Therefore, we could conclude that mimicking glaucomatous conditions in a cell model reduces the expression of D₃-MT₁ and D₃-MT₂ heteroreceptor complexes.

Finally, exploratory experiments on heteromer expression were performed in the postmortem samples obtained from glaucoma patients and age-matched controls. Given the limited availability of these unique samples, which in part reflects ethical issues, we had access to two control (healthy) and two glaucomatous eyes. Accordingly, statistical analysis could not be performed on the results described below. PLA was performed in ciliary body sections of glaucoma patients and age-matched controls. In the samples from normotensive eyes, marked expression of D₃R–MT₁R and D₃R–MT₂R heteromers was found in the basal membrane of the non-pigmented epithelium. No heteromer expression was found in the stroma of the ciliary processes (Figure 5A,D). A negligible PLA signal was found in the negative controls performed by omitting one of the primary antibodies (Figure 5C). When samples from glaucoma cases were analyzed, we observed a significant reduction in the number dots for both heteromers (Figure 5B,E), with up to a 50% reduction in D₃R–MT₁R heteromer expression and a reduction of up to 45% in the case of D₃R–MT₂R heteromers (Figure 5F). Together with the results obtained in the 59HCE cells, these data point to a reduction of dopamine–melatonin heteroreceptor complexes under conditions of elevated intraocular pressure.

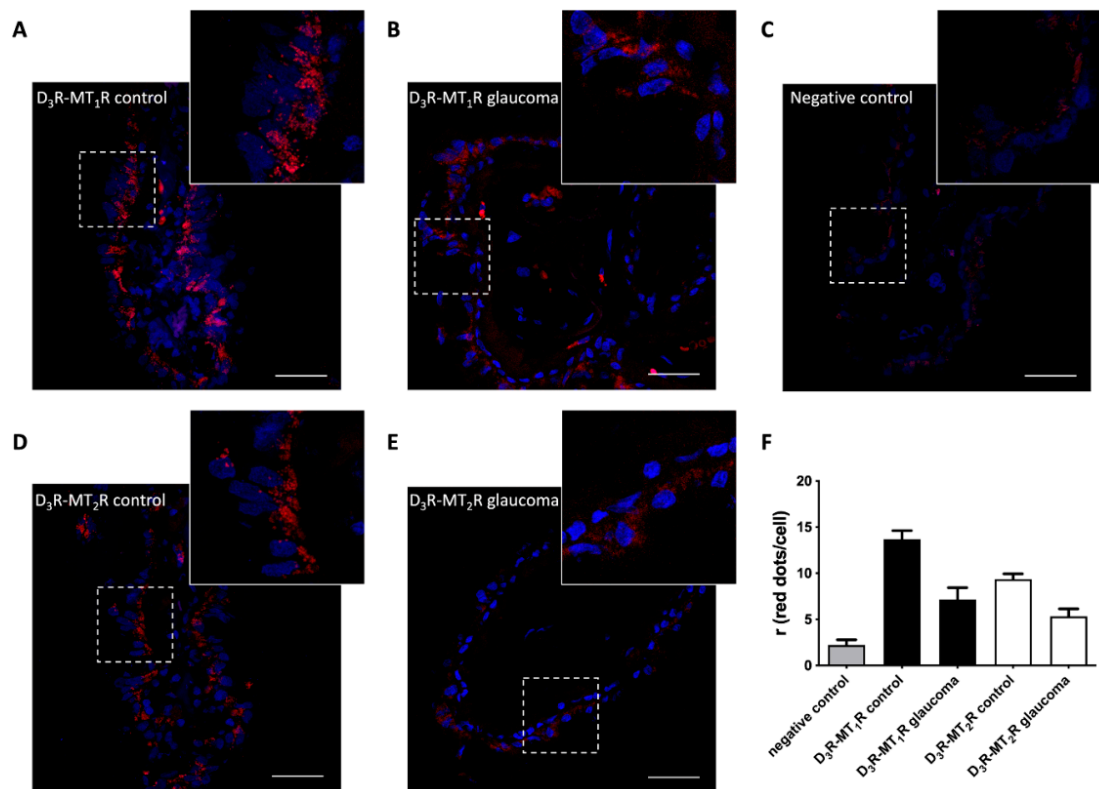


Figure 5. D₃-MT₁ and D₃-MT₂ receptor heteromer expression in the human ciliary body. In situ proximity ligation assays were performed as described in Materials and Methods using human ciliary body sections from age-matched intraocular pressure (IOP) normotensive individuals (control) (A,C,D)

and glaucoma patients (B,E). Confocal microscopy images (superimposed sections) are shown. D₃-MT₁ (A,B) and D₃-MT₂ (D,E) receptor heteromers appear as red clusters and Hoechst-stained nuclei appear in blue. (C) A negative control obtained by omitting one of the primary antibodies is shown. The ratio (number of red spots/cell) for the indicated samples is shown in (F). Data are the mean ± S.E.M. of counts in 6 different fields (each image covered an area of 238 μm²) from every sample from the controls (n = 2) or glaucoma patients (n = 2). Scale bar: 40 μm.

4. Discussion

Dopamine, one of the primary neurotransmitters of the central nervous system, participates in almost any higher-order function, from motor control to emotion control, and from cognition to behavior. Dopamine is also a neurohormone acting in the periphery via the same receptors that are expressed in the brain. The difference is that the relevant actions of dopamine are mainly exerted by neuronal receptors, while in the periphery, these receptors are expressed in almost any kind of cell type. A prospective study, made in our laboratory, showed the expression of the D₃R in different cells of the eye structure, including those that controlled IOP. These expression results fit with pharmacological studies showing that different D₃R agonists may lower IOP and that the effect is lost in D₃R^{-/-} mice [43–45]. From earlier studies by the laboratory of S. George [55–57] it is known that dopamine receptors may directly interact with themselves to form homodimers or with other GPCRs. In a previous study, we also discovered D₁-D₃ heteroreceptor complexes with high relevance in Parkinson's disease-associated dyskinesia [53]. For these reasons, we explored whether the D₃R expressed in ocular structures could form functional heteromers with other GPCR of significant relevance for eye physiology.

Melatonin is an example of a neurohormone produced by the pineal gland that may also be produced (and released) elsewhere. Enzymes that participate in the synthesis of melatonin are expressed in different cell types and the indoleamine participates in IOP regulation. Although the retina was among the first identified structures able to synthesize melatonin [58,59], other eye cell types express melatonin synthesizing enzymes (see 1. Introduction).

Our results decipher one of the mechanisms underlying the dopamine–melatonin interactions described to occur in the eye. Based on prototypic heteromer prints that occur similarly in heterologous expression systems and natural cell lines, and by further confirmation in natural sources by PLA, we discovered novel physiologically relevant receptor–receptor interactions. The D₃R, expressed in ciliary body epithelial cells, may interact with either MT₁R or MT₂R. Canonical coupling of melatonin receptors individually expressed in a heterologous system is to Gi (see References [25,52] and references therein). Dopamine receptors are either coupled to Gs (D₁ and D₅) or Gi (D₂, D₃ and D₄). Remarkably, in the D₃R–MT₁R and the D₃R–MT₂R heteromer, the dopamine receptor did not couple to Gi but was still functional, as dopamine receptor agonists could activate the MAPK pathway. Indeed, heteromerization produced a biased functionality, i.e., a given agonist of the D₃R, e.g., 7-OH-PIPAT may engage Gi-mediated signaling but only in the right context [60]. Our results prove antagonistic interactions, thus constituting a base to understand why the levels of dopamine and melatonin in the eye are oppositely varying according to the 24-h circadian rhythm [39,40]. Not only the presence of melatonin receptors and heteromer formation alters D₃R-mediated signaling, but coactivation of receptors—in heteromers—by moderate levels of the indoleamine and of dopamine would result in a decrease in the overall signal transduction output. Accordingly, these heteromers mediate dopamine/melatonin antagonistic actions in the eye.

Considering IOP regulation by melatonin, circadian rhythms, and opposite melatonin/dopamine circadian levels in the eye; the results of heteromer expression in both a cell model of eye-related hypertension, namely 59HCE cells treated with a TRPV4 agonist, and the human eye (from IOP normotensive and hypertensive individuals) were relevant. They provided evidence of a correlation between heteromer D₃R–MT₁R and D₃R–MT₂R complex disruption and elevated IOP. Despite the few studies addressing GPCR heteromer expression in disease, often the results are quite relevant.

On the one hand, they provide the basis for confirming whether the heteromer is expressed or not and, accordingly, whether the heteromer may be a therapeutic target. On the other hand, the differential functionality may lead to understanding of the consequences, at the signaling level, of the maintenance or the disassembly of heteroreceptor complexes. This will provide reliable information on the pathophysiology and factors affecting the course of the disease.

Based on our results, we think that future directions should include interventions assaying IOP after infusions in the eye of a combination of melatonin and either D₃R agonists or antagonists at different times of the day in wild type animals and in a glaucoma animal model, such as the aged DBA/2J mice [61,62]. From the results of such analysis, a potential therapy would arise for the assessment of the hypertensive eye.

Author Contributions: Conceptualization, H.A.A., J.P., G.N., and R.F.; data curation, I.R.-R. and G.N.; Formal analysis, I.R.-R. and A.d.S.-B.; Funding acquisition, J.P. and R.F.; Investigation, I.R.-R., J.L., G.N., and A.d.S.-B.; Methodology, I.R.-R., H.A.A., J.L., J.J., J.P., G.N., and R.F.; Project administration, J.J., J.P., and R.F.; Resources, J.S.-N., J.P. and R.F. Supervision, J.P. G.N., and R.F.; Validation, J.P. G.N. and R.F.; Visualization, J.P. G.N., and R.F.; Writing—original draft, I.R.-R. H.A.A., and R.F.; Writing—review & editing, I.R.-R., H.A.A., G.N., and R.F. All authors (except J.P., see Acknowledgements) have read and validated the submitted version. All authors (except J.P.) have read and agreed to the published version of the manuscript.

Funding: This research was funded by grants from the Spanish Ministerio de Economía y Competitividad (MINECO) Ref. [SAF2013-44416-R], [SAF2016-77084-R] and [BFU2015-64405-R], and from the Spanish Ministerio de Sanidad Ref. RETICS [RD12/0034/0003] and [RD16/0008/0017]. Hanan A. Alkozi is a fellowship holder of the Saudi Arabian government. MINECO grants may include EU FEDER funds. The “NBM” Molecular Neurobiology laboratory of the University of Barcelona is considered of excellence (“*grup consolidat*”) by the regional Catalanian Government, which neither provides funds to the consolidated laboratory nor to perform the research here reported.

Acknowledgments: In memoriam of our co-author Jesús Pintor, astounding as a scientist and yet a good person.

Conflicts of Interest: The authors declare no conflict of interest.

Appendix A

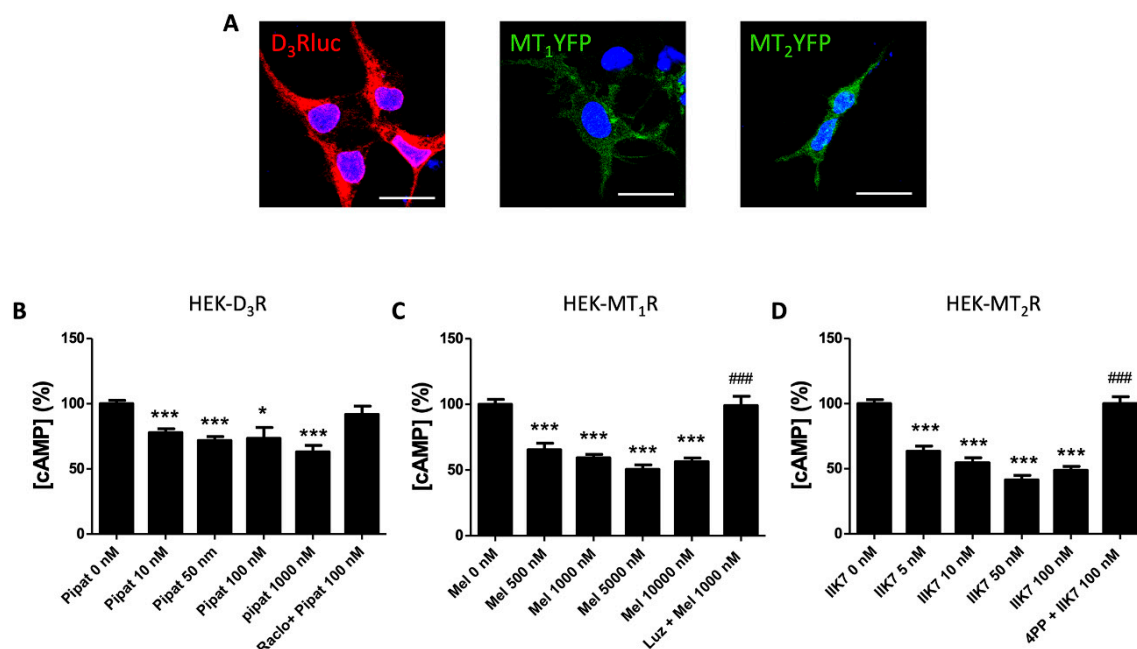


Figure A1. Membrane receptor expression and cAMP responses in single-transfected HEK-293T cells. (A) Confocal microscopy images of HEK-293T cells transfected with cDNAs for D₃R-Rluc (2 µg), MT₁R-YFP (2 µg), or MT₂R-YFP (2 µg). D₃ receptors (red) were identified by immunocytochemistry using anti-Rluc antibodies. MT₁ and MT₂ receptors (green) were identified from the fluorescence of YFP-containing fusion proteins. Cell nuclei were stained with Hoechst (blue channel). Scale bar:

20 μm . Panels (B–D) HEK-293T cells transfected with cDNAs encoding for D₃R (1.5 μg) (B), MT₁R (1.5 μg) (C) or MT₂R (1.5 μg) (D) cells were pre-treated with vehicle or antagonists (1 μM raclopride for D₃R, 1 μM luzindole for MT₁R or 1 μM 4PPDOT for MT₂R), and then subsequently treated with different concentrations of selective agonists (10–1000 nM 7-OH-PIPAT for D₃R, 0.5–10 μM melatonin for MT₁R or 5–100 nM IIK7 for MT₂R). cAMP accumulation was detected by TR-FRET in the presence of 0.5 μM forskolin. cAMP production is expressed as % of levels obtained by 0.5 μM forskolin (0 nM agonist). Values are the mean \pm S.E.M. of 6 different experiments performed in triplicates, and one-way ANOVA followed by Bonferroni's multiple comparison post-hoc tests were used for statistical analysis. (* $p < 0.05$, *** $p < 0.001$; versus treatment with forskolin). (### $p < 0.001$; versus treatment with 1 μM melatonin or 100 nM IIK7 alone).

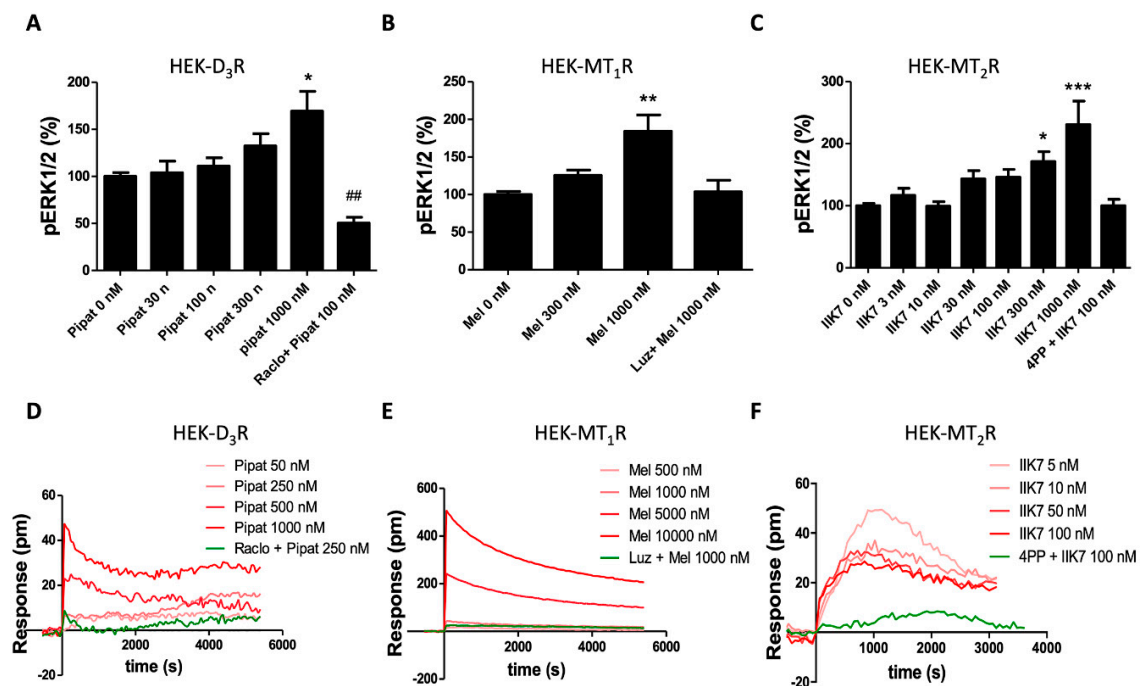


Figure A2. ERK phosphorylation and DMR responses in single-transfected HEK-293T cells. HEK-293T cells transfected with cDNA encoding for D₃R (1.5 μg) (A,D), MT₁R (1.5 μg) (B,E), or MT₂R (1.5 μg) (C,F) were pre-treated with vehicle or antagonists (1 μM raclopride for D₃R, 1 μM luzindole for MT₁R, or 1 μM 4PPDOT for MT₂R), and then subsequently treated with different concentrations of agonists (30–1000 nM 7-OH-PIPAT for D₃R, 0.3–10 μM melatonin for MT₁R, or 3–1000 nM IIK7 for MT₂R). ERK1/2 phosphorylation (A–C) was analyzed using an AlphaScreen[®]SureFire[®] kit (Perkin Elmer). ERK1/2 phosphorylation data are expressed as % with respect to basal levels (0 nM agonist). Values are the mean \pm S.E.M. of seven different experiments performed in triplicates, and one-way ANOVA followed by Bonferroni's multiple comparison post-hoc tests were used for statistical analysis. (* $p < 0.05$, ** $p < 0.01$, *** $p < 0.001$; versus basal). (## $p < 0.001$; versus treatment with 100 nM 7-OH-PIPAT alone). (D–F) DMR tracings representing the picometer-shifts of reflected light wavelengths over time upon agonist ligand treatment.

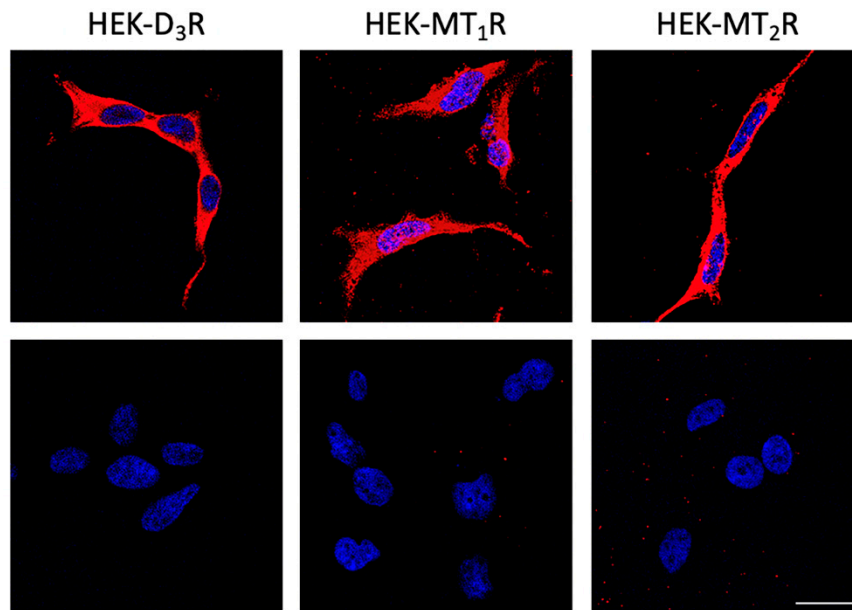


Figure A3. The specificity of antibodies against D₃, MT₁, and MT₂ receptors. Confocal microscopy images of the HEK-293T cells untransfected (bottom) or transfected with cDNAs coding for D₃, MT₁, or MT₂ receptors (0.5 µg). The cells were treated with primary antibodies against either D₃, MT₁, or MT₂ receptors (as indicated), and subsequently treated with a Cy3 secondary antibody (red). Images were taken near the bottom of the cell and, therefore, reflect the labeling in the membrane in contact with the slide. Cell nuclei were stained with Hoechst (blue channel). Scale bar: 20 µm.

References

1. Delamere, N.A. Ciliary Body and Ciliary Epithelium. *Adv. Organ. Biol.* **2005**, *10*, 127–148. [[PubMed](#)]
2. Tamm, E.R.; Lütjen-Drecoll, E. Ciliary body. *Microsc. Res. Tech.* **1996**, *33*, 390–439. [[CrossRef](#)]
3. Civan, M.M.; Macknight, A.D.C. The ins and outs of aqueous humour secretion. *Exp. Eye Res.* **2004**, *78*, 625–631. [[CrossRef](#)]
4. Adler, F.H. Is the Aqueous Humor a Dialysate? *Trans. Am. Ophthalmol. Soc.* **1933**, *31*, 131–142. [[CrossRef](#)] [[PubMed](#)]
5. Davson, H.; Duke-Elder, W.S.; Benham, G.H. The ionic equilibrium between the aqueous humour and blood plasma of cats. *Biochem. J.* **1936**, *30*, 773–775. [[CrossRef](#)] [[PubMed](#)]
6. Krupin, T.; Wax, M.; Moolchandani, J. Aqueous production. *Trans. Ophthalmol. Soc. U. K.* **1986**, *105*, 156–161. [[PubMed](#)]
7. Casson, R.J.; Chidlow, G.; Wood, J.P.M.; Crowston, J.G.; Goldberg, I. Definition of glaucoma: Clinical and experimental concepts. *Clin. Experiment. Ophthalmol.* **2012**, *40*, 341–349. [[CrossRef](#)]
8. McCannel, C.A.; Heinrich, S.R.; Brubaker, R.F. Acetazolamide but not timolol lowers aqueous humor flow in sleeping humans. *Graefe's Arch. Clin. Exp. Ophthalmol.* **1992**, *230*, 518–520. [[CrossRef](#)]
9. Asrani, S.; Zeimer, R.; Wilensky, J.; Gieser, D.; Vitale, S.; Lindenmuth, K. Large diurnal fluctuations in intraocular pressure are an independent risk factor in patients with glaucoma. *J. Glaucoma* **2000**, *9*, 134–142. [[CrossRef](#)]
10. Lerner, A.B.; Case, J.D.; Takahashi, Y. Isolation of melatonin and 5-methoxyindole-3-acetic acid from bovine pineal glands. *J. Biol. Chem.* **1960**, *235*, 1992–1997.
11. Arendt, J. Jet-lag and shift work: (2) Therapeutic use of melatonin. *J. R. Soc. Med.* **1999**, *92*, 402–405. [[CrossRef](#)] [[PubMed](#)]
12. Sánchez-Barceló, E.J.; Mediavilla, M.D.; Tan, D.X.; Reiter, R.J. Clinical uses of melatonin: Evaluation of human trials. *Curr. Med. Chem.* **2010**, *17*, 2070–2095. [[CrossRef](#)] [[PubMed](#)]
13. Pang, S.F.; Yu, H.S.; Suen, H.C.; Brown, G.M. Melatonin in the retina of rats: A diurnal rhythm. *J. Endocrinol.* **1980**, *87*, 89–93. [[CrossRef](#)] [[PubMed](#)]

14. Aimoto, T.; Rohde, B.H.; Chiou, G.C.; Lauber, J.K. N-acetyltransferase activity and melatonin level in the eyes of glaucomatous chickens. *J. Ocul. Pharmacol.* **1985**, *1*, 149–160. [[CrossRef](#)]
15. Abe, M.; Itoh, M.T.; Miyata, M.; Shimizu, K.; Sumi, Y. Circadian rhythm of serotonin N-acetyltransferase activity in rat lens. *Exp. Eye Res.* **2000**, *70*, 805–808. [[CrossRef](#)]
16. Quay, W.B. Increases in Volume, Fluid Content, and Lens Weight of Eyes Following Systemic Administration of Melatonin. *J. Pineal Res.* **1984**, *1*, 3–13. [[CrossRef](#)]
17. Djeridane, Y.; Vivien-Roels, B.; Simonneaux, V.; Miguez, J.M.; Pévet, P. Evidence for melatonin synthesis in rodent Harderian gland: A dynamic in vitro study. *J. Pineal Res.* **1998**, *25*, 54–64. [[CrossRef](#)]
18. Mhatre, M.C.; van Jaarsveld, A.S.; Reiter, R.J. Melatonin in the lacrimal gland: First demonstration and experimental manipulation. *Biochem. Biophys. Res. Commun.* **1988**, *153*, 1186–1192. [[CrossRef](#)]
19. Reppert, S.M.; Weaver, D.R.; Ebisawa, T. Cloning and characterization of a mammalian melatonin receptor that mediates reproductive and circadian responses. *Neuron* **1994**, *13*, 1177–1185. [[CrossRef](#)]
20. Reppert, S.M.; Godson, C.; Mahle, C.D.; Weaver, D.R.; Slaugenhaupt, S.A.; Gusella, J.F. Molecular characterization of a second melatonin receptor expressed in human retina and brain: The Mel1b melatonin receptor. *Proc. Natl. Acad. Sci. USA* **1995**, *92*, 8734–8738. [[CrossRef](#)]
21. Li, D.Y.; Smith, D.G.; Hardeland, R.; Yang, M.Y.; Xu, H.L.; Zhang, L.; Yin, H.D.; Zhu, Q. Melatonin receptor genes in vertebrates. *Int. J. Mol. Sci.* **2013**, *14*, 11208–11223. [[CrossRef](#)] [[PubMed](#)]
22. Crooke, A.; Guzman-Aranguez, A.; Mediero, A.; Alarma-Estrany, P.; Carracedo, G.; Pelaez, T.; Peral, A.; Pintor, J. Effect of Melatonin and Analogues on Corneal Wound Healing: Involvement of Mt₂ Melatonin Receptor. *Curr. Eye Res.* **2015**, *40*, 56–65. [[CrossRef](#)] [[PubMed](#)]
23. Xue, K.-C.; Hu, D.-D.; Zhao, L.; Li, N.; Shen, H.-Y. Correlation between presence of primary iris- and ciliary body cysts and intraocular pressure. *Eur. Rev. Med. Pharmacol. Sci.* **2017**, *21*, 3985–3989. [[PubMed](#)]
24. Bietti, G. Surgical intervention on the ciliary body: New Trends for the Relief of Glaucoma. *J. Am. Med. Assoc.* **1950**, *142*, 889–897. [[CrossRef](#)] [[PubMed](#)]
25. Cardinali, D.P.; Delagrange, P.; Dubocovich, M.L.; Jockers, R.; Krause, D.N.; Markus, R.P.; Olcese, J.; Pintor, J.; Renault, N.; Sugden, D.; et al. Melatonin receptors (version 2019.4) in the IUPHAR/BPS Guide to Pharmacology Database. *IUPHAR/BPS Guid. to Pharmacol. CITE* **2019**, *2019*. [[CrossRef](#)]
26. Alexander, S.P.; Christopoulos, A.; Davenport, A.P.; Kelly, E.; Marrion, N.V.; Peters, J.A.; Faccenda, E.; Harding, S.D.; Pawson, A.J.; Sharman, J.L.; et al. CGTP Collaborators The concise guide to Pharmacology 2017/18: G protein-coupled receptors. *Br. J. Pharmacol.* **2017**, *174*, S17–S129. [[CrossRef](#)]
27. Von Gall, C.; Weaver, D.R.; Kock, M.; Korf, H.W.; Stehle, J.H. Melatonin limits transcriptional impact of phosphoCREB in the mouse SCN via the Mel1a receptor. *Neuroreport* **2000**, *11*, 1803–1807. [[CrossRef](#)]
28. Brydon, L.; Roka, F.; Petit, L.; De Coppet, P.; Tissot, M.; Barrett, P.; Morgan, P.J.; Nanoff, C.; Strosberg, A.D.; Jockers, R. Dual signaling of human Mel1a melatonin receptors via G_{i2}, G_{i3}, and G_{q/11} proteins. *Mol. Endocrinol.* **1999**, *13*, 2025–2038. [[CrossRef](#)]
29. Pandi-Perumal, S.R.; Trakht, I.; Srinivasan, V.; Spence, D.W.; Maestroni, G.J.M.; Zisapel, N.; Cardinali, D.P. Physiological effects of melatonin: Role of melatonin receptors and signal transduction pathways. *Prog. Neurobiol.* **2008**, *85*, 335–353. [[CrossRef](#)]
30. Huete-Toral, F.; Crooke, A.; Martínez-Águila, A.; Pintor, J.; Martínez-Aguila, A.; Pintor, J.; Martínez-Águila, A.; Pintor, J. Melatonin receptors trigger cAMP production and inhibit chloride movements in nonpigmented ciliary epithelial cells. *J. Pharmacol. Exp. Ther.* **2015**, *352*, 119–128. [[CrossRef](#)]
31. Cecon, E.; Oishi, A.; Jockers, R. Melatonin receptors: Molecular pharmacology and signalling in the context of system bias. *Br. J. Pharmacol.* **2017**, *175*, 3263–3280. [[CrossRef](#)] [[PubMed](#)]
32. Levoye, A.; Dam, J.; Ayoub, M.A.; Guillaume, J.L.; Couturier, C.; Delagrange, P.; Jockers, R. The orphan GPR50 receptor specifically inhibits MT1 melatonin receptor function through heterodimerization. *EMBO J.* **2006**, *25*, 3012–3023. [[CrossRef](#)] [[PubMed](#)]
33. Kamal, M.; Gbahou, F.; Guillaume, J.-L.; Daulat, A.M.; Benleulmi-Chaachoua, A.; Luka, M.; Chen, P.; Kalbasi Anaraki, D.; Baroncini, M.; Mannoury la Cour, C.; et al. Convergence of melatonin and serotonin (5-HT) signaling at MT2/5-HT2C receptor heteromers. *J. Biol. Chem.* **2015**, *290*, 11537–11546. [[CrossRef](#)] [[PubMed](#)]
34. Alkozi, H.A.; Navarro, G.; Aguinaga, D.; Reyes-Resina, I.; Sanchez-Naves, J.; de Lara, M.J.P.; Franco, R.; Pintor, J. Adrenergic-melatonin heteroreceptor complexes are key in controlling ion homeostasis and intraocular eye pressure and their disruption contributes to hypertensive glaucoma. *bioRxiv* **2019**, 636688. [[CrossRef](#)]

35. Cahill, G.M.; Besharse, J.C. Resetting the circadian clock in cultured *Xenopus* eyecups: Regulation of retinal melatonin rhythms by light and D2 dopamine receptors. *J. Neurosci.* **1991**, *11*, 2959–2971. [[CrossRef](#)] [[PubMed](#)]
36. Iuvone, P.M.; Besharse, J.C. Dopamine receptor-mediated inhibition of serotonin N-acetyltransferase activity in retina. *Brain Res.* **1986**, *369*, 168–176. [[CrossRef](#)]
37. Iuvone, P.M.; Besharse, J.C. Cyclic AMP stimulates serotonin N-acetyltransferase activity in *Xenopus* retina in vitro. *J. Neurochem.* **1986**, *46*, 33–39. [[CrossRef](#)] [[PubMed](#)]
38. Ivanova, T.N.; Alonso-Gomez, A.L.; Iuvone, P.M. Dopamine D4 receptors regulate intracellular calcium concentration in cultured chicken cone photoreceptor cells: Relationship to dopamine receptor-mediated inhibition of cAMP formation. *Brain Res.* **2008**, *1207*, 111–119. [[CrossRef](#)] [[PubMed](#)]
39. Adachi, A.; Nogi, T.; Ebihara, S. Phase-relationship and mutual effects between circadian rhythms of ocular melatonin and dopamine in the pigeon. *Brain Res.* **1998**, *792*, 361–369. [[CrossRef](#)]
40. Adachi, A.; Suzuki, Y.; Nogi, T.; Ebihara, S. The relationship between ocular melatonin and dopamine rhythms in the pigeon: Effects of melatonin inhibition on dopamine release. *Brain Res.* **1999**, *815*, 435–440. [[CrossRef](#)]
41. Zawilska, J.B.; Nowak, J.Z. Dopamine D4-like receptors in vertebrate retina: Does the retina offer a model for the D4-receptor analysis? *Pol. J. Pharmacol.* **1997**, *49*, 201–211.
42. Caravaggio, F.; Scifo, E.; Sibille, E.L.; Hernandez-Da Mota, S.E.; Gerretsen, P.; Remington, G.; Graff-Guerrero, A. Expression of dopamine D2 and D3 receptors in the human retina revealed by positron emission tomography and targeted mass spectrometry. *Exp. Eye Res.* **2018**, *175*, 32–41. [[CrossRef](#)]
43. Pescosolido, N.; Parisi, F.; Russo, P.; Buomprisco, G.; Nebbioso, M. Role of dopaminergic receptors in glaucomatous disease modulation. *Biomed. Res. Int.* **2013**, *2013*, 193048. [[CrossRef](#)] [[PubMed](#)]
44. Chu, E.; Socci, R.; Chu, T.-C. PD128,907 induces ocular hypotension in rabbits: Involvement of D2/D3 dopamine receptors and brain natriuretic peptide. *J. Ocul. Pharmacol. Ther.* **2004**, *20*, 15–23. [[CrossRef](#)] [[PubMed](#)]
45. Chu, E.; Chu, T.C.; Potter, D.E. Mechanisms and sites of ocular action of 7-hydroxy-2-dipropylaminotetralin: A dopamine₃ receptor agonist. *J. Pharmacol. Exp. Ther.* **2000**, *293*, 710–716. [[PubMed](#)]
46. Curtis, M.J.; Alexander, S.; Cirino, G.; Docherty, J.R.; George, C.H.; Giembycz, M.A.; Hoyer, D.; Insel, P.A.; Izzo, A.A.; Ji, Y.; et al. Experimental design and analysis and their reporting II: Updated and simplified guidance for authors and peer reviewers. *Br. J. Pharmacol.* **2018**, *175*, 987–993. [[CrossRef](#)]
47. Alexander, S.P.H.; Roberts, R.E.; Broughton, B.R.S.; Sobey, C.G.; George, C.H.; Stanford, S.C.; Cirino, G.; Docherty, J.R.; Giembycz, M.A.; Hoyer, D.; et al. Goals and practicalities of immunoblotting and immunohistochemistry: A guide for submission to the British Journal of Pharmacology. *Br. J. Pharmacol.* **2018**, *175*, 407–411. [[CrossRef](#)]
48. Sugden, D.; Yeh, L.K.; Teh, M.T. Design of subtype selective melatonin receptor agonists and antagonists. In *Reproduction Nutrition Development*; Elsevier Masson SAS: Paris, France, 1999; Volume 39, pp. 335–344.
49. Martínez-Pinilla, E.; Varani, K.; Reyes-Resina, I.; Angelats, E.; Vincenzi, F.; Ferreiro-Vera, C.; Oyarzabal, J.; Canela, E.I.; Lanciego, J.L.; Nadal, X.; et al. Binding and signaling studies disclose a potential allosteric site for cannabidiol in cannabinoid CB2 receptors. *Front. Pharmacol.* **2017**, *8*, 744. [[CrossRef](#)]
50. Navarro, G.; Borroto-Escuela, D.; Angelats, E.; Etayo, I.; Reyes-Resina, I.; Pulido-Salgado, M.; Rodríguez-Pérez, A.; Canela, E.; Saura, J.; Lanciego, J.L.; et al. Receptor-heteromer mediated regulation of endocannabinoid signaling in activated microglia. Role of CB1 and CB2 receptors and relevance for Alzheimer’s disease and levodopa-induced dyskinesia. *Brain Behav. Immun.* **2018**, *67*, 139–151. [[CrossRef](#)]
51. Hinz, S.; Navarro, G.; Borroto-Escuela, D.; Seibt, B.F.; Ammon, C.; De Filippo, E.; Danish, A.; Lacher, S.K.; Červinková, B.; Rafehi, M.; et al. Adenosine A2A receptor ligand recognition and signaling is blocked by A2B receptors. *Oncotarget* **2018**, *9*, 13593–13611. [[CrossRef](#)]
52. Rivas-Santisteban, R.; Reyes-Resina, I.; Raich, I.; Pintor, J.J.; Alkozi, H.A.; Navarro, G.; Franco, R. Specificity and nanomolar potency of melatonin on G-protein coupled melatonin MT1 and MT2 receptors expressed in HEK-293T human embryo kidney cells. *Melatonin Res.* **2019**, *2*, 121–131. [[CrossRef](#)]
53. Marcellino, D.; Ferré, S.; Casadó, V.; Cortés, A.; Le Foll, B.; Mazzola, C.; Drago, F.; Saur, O.; Stark, H.; Soriano, A.; et al. Identification of dopamine D1–D3 receptor heteromers: Indications for a role of synergistic D1–D3 receptor interactions in the striatum. *J. Biol. Chem.* **2008**, *283*, 26016–26025. [[CrossRef](#)]

54. Alkozi, H.A.; Perez de Lara, M.J.; Sánchez-Naves, J.; Pintor, J. TRPV4 Stimulation Induced Melatonin Secretion by Increasing Arylalkylamine N-acetyltransferase (AANAT) Protein Level. *Int. J. Mol. Sci.* **2017**, *18*, 746. [[CrossRef](#)] [[PubMed](#)]
55. Ng, G.Y.K.; O'Dowd, B.F.; Lee, S.P.; Chung, H.T.; Brann, M.R.; Seeman, P.; George, S.R. Dopamine D2 receptor dimers and receptor-blocking peptides. *Biochem. Biophys. Res. Commun.* **1996**, *227*, 200–204. [[CrossRef](#)] [[PubMed](#)]
56. Lee, S.P.; So, C.H.; Rashid, A.J.; Varghese, G.; Cheng, R.; Lança, A.J.; O'Dowd, B.F.; George, S.R. Dopamine D1 and D2 receptor Co-activation generates a novel phospholipase C-mediated calcium signal. *J. Biol. Chem.* **2004**, *279*, 35671–35678. [[CrossRef](#)] [[PubMed](#)]
57. Perreault, M.L.; Hasbi, A.; Alijaniam, M.; Fan, T.; Varghese, G.; Fletcher, P.J.; Seeman, P.; O'Dowd, B.F.; George, S.R. The dopamine D1-D2 receptor heteromer localizes in dynorphin/enkephalin neurons: Increased high affinity state following amphetamine and in schizophrenia. *J. Biol. Chem.* **2010**, *285*, 36625–36634. [[CrossRef](#)] [[PubMed](#)]
58. Huang, H.; Wang, Z.; Weng, S.J.; Sun, X.H.; Yang, X.L. Neuromodulatory role of melatonin in retinal information processing. *Prog. Retin. Eye Res.* **2013**, *32*, 64–87. [[CrossRef](#)] [[PubMed](#)]
59. Nagle, C.A.; Cardinali, D.P.; Rosner, J.M. Retinal and pineal hydroxyindole-O-methyl transferases in the rat: Changes following cervical sympathectomy, pinealectomy or blinding. *Endocrinology* **1973**, *92*, 1560–1564. [[CrossRef](#)] [[PubMed](#)]
60. Franco, R.; Aguinaga, D.; Jiménez, J.; Lillo, J.; Martínez-Pinilla, E.; Navarro, G. Biased receptor functionality versus biased agonism in G-protein-coupled receptors. *Biomol. Concepts* **2018**, *9*, 143–154. [[CrossRef](#)]
61. Pérez de Lara, M.J.; Santano, C.; Guzmán-Aránguez, A.; Valiente-Soriano, F.J.; Avilés-Trigueros, M.; Vidal-Sanz, M.; de la Villa, P.; Pintor, J. Assessment of inner retina dysfunction and progressive ganglion cell loss in a mouse model of glaucoma. *Exp. Eye Res.* **2014**, *122*, 40–49. [[CrossRef](#)]
62. John, S.W.M.; Smith, R.S.; Savinova, O.V.; Hawes, N.L.; Chang, B.; Turnbull, D.; Davisson, M.; Roderick, T.H.; Heckenlively, J.R. Essential iris atrophy, pigment dispersion, and glaucoma in DBA/2J mice. *Investig. Ophthalmol. Vis. Sci.* **1998**, *39*, 951–962.



© 2020 by the authors. Licensee MDPI, Basel, Switzerland. This article is an open access article distributed under the terms and conditions of the Creative Commons Attribution (CC BY) license (<http://creativecommons.org/licenses/by/4.0/>).